

# Structural and optical properties of ZnSe thin films stacked with PbSe submonolayers

M. Manonmani Parvathi · V. Arivazhagan · S. Rajesh

Received: 9 May 2013 / Accepted: 17 February 2014 / Published online: 5 March 2014  
© Springer-Verlag Berlin Heidelberg 2014

**Abstract** Structural and optical properties of Zinc Selenide (ZnSe) thin films stacked with multiple Lead Selenide (PbSe) submonolayers (ML) were studied. Thermal evaporation was preferred to produce ZnSe–PbSe thin films with the PbSe ML thickness ranges from 2.5 to 10 nm. Polycrystalline nature of the ZnSe was revealed through high resolution X-ray diffractometer measurement. The development of micro strain at the interfaces with increasing PbSe ML thickness was observed. A cross-sectional TEM image shows well-ordered periodicity and reproducibility of the layer thickness. The enhancement of optical absorption of ZnSe was identified upon stacking of PbSe ML. The evidence for quantum confinement in PbSe ML was revealed by the obtained red shift in band gap (2.5–1.8 eV) values as well as photoluminescence emission at 1,071 nm. The presence of tensile strain in the ZnSe layers upon staking of PbSe ML was discussed by the shift in LO phonon modes in Raman spectra.

## 1 Introduction

Zinc Selenide (ZnSe) attracts considerable attention due to its interesting structural, optical, and electrical properties that can be useful in multiple fields in solid state device technologies. It has been proposed for improving in many devices such as in solar cells, green–blue light emitting diodes, photo detectors etc. [1–5]. A large portion of these devices are fabricated using thin film technology such as

vacuum deposition, sputtering, electrodeposition, pulsed laser deposition etc. [2–8]. The application of ZnSe in optoelectronics arises from its wide band gap (2.6 eV), large exciton binding energy of 21 meV, small Bohr radius of 4.5 nm, and transparency in visible spectrum. In past years, a wide knowledge of research works have been done on ZnSe by changing several parameters such as temperature, dopants, composition, substrates, multilayers, and heterostructures [9–12]. All the reports show a dramatic feature in its fundamental properties like absorption at visible region. However, ZnSe with narrow band gap material composition leads to enhance as well as modify the structural and optical behaviour. It is well known that IV–VI group semiconductor of Lead Selenide (PbSe) has gained a great deal of attention over the last decades due to its remarkable notification towards high conversion efficient solar cells, because it offers multiple exciton generation and fast hot electron transport [13, 14]. However, PbSe is very active in low energy region of electromagnetic spectrum and combining this with the wide band gap and functional materials are effective in current research. Yun et al. [1] reported enhanced optical absorption of polymer–ZnSe composite with introducing PbSe nanocrystals in hybrid photovoltaic solar cells. Abe [6] has reported that the enhanced optical absorption in desirable energy range for solar cell application for PbSe–ZnSe composite thin film. Lack of literature on ZnSe–PbSe compound or heterostructure is a key for the present work. In this work, we report ZnSe thin films stacked with PbSe submonolayers (ML) of thickness ranges from 2.5 to 10 nm. Structural and optical properties of ZnSe thin films with PbSe ML are reported. Result shows that the enhanced absorption at visible region in the electromagnetic spectrum associated with the ZnSe along with emission at NIR region due to the quantum confined 2D layers of stacked PbSe ML. In

M. Manonmani Parvathi · V. Arivazhagan · S. Rajesh (✉)  
Department of Physics, Karunya University,  
Coimbatore 641 114, India  
e-mail: drsrajesh@karunya.edu

addition, crystal structure by means of X-ray diffraction and laser Raman scattering is being investigated. The obtained results are compared to those reported on ZnSe thin films, to confirm the primary contribution of carrier confinement of PbSe phase in ZnSe thin films.

## 2 Experiment

A vacuum deposition technique was used to prepare ZnSe–PbSe compound thin films on ultrasonically cleaned glass substrates and on Si wafer (for TEM analysis) kept at room temperature. The room temperature of the vacuum chamber was maintained using a cooling system with water. A high purity PbSe ingot and ZnSe powder (both from Sigma Aldrich, 99.99 %) were placed in two individual molybdenum boats. Initially, ZnSe was deposited on the substrate with a thickness of 100 nm. Then a PbSe ML was deposited with a thickness of 2.5 nm (17 times less than its Bohr radius) followed by a 25 nm ZnSe layer at a vacuum of  $10^{-6}$  torr. The cycle was repeated for five such pairs of ZnSe–PbSe ML without breaking the vacuum. The ZnSe–PbSe ML structure was prepared with various PbSe ML thicknesses ranging from 2.5 to 10 nm with the increment of 2.5 nm, while the bottom and interlayers thicknesses of ZnSe were maintained as 100 and 25 nm, respectively, in all the structures. The layer thicknesses were monitored and controlled using an in situ quartz crystal thickness monitor. The structural analysis was carried out using PANalytical (PW3040/60) high resolution X-ray diffractometer (HRXRD) using Cu- $K\alpha$  radiation with the range of  $2\theta$  between  $20^\circ$  and  $60^\circ$ . The cross-sectional TEM image was taken by JEOL 2010F Transmission electron microscopy operating at 200 kV in bright field mode. Cross-sectional TEM samples were prepared using a Gatan PIPS ion mill using focussed  $\text{Ar}^+$  ion beam milling. The optical absorption spectra were recorded using a UV–VIS–NIR spectrophotometer (Jasco-570) in the wavelength range of 200–2,500 nm. Room temperature Photoluminescence analysis was carried out with a photoluminescence (PL) setup using 532 nm continuous lasers with the beam spot of 1  $\mu\text{m}$ . Raman scattering was done using LabRAM HR 800 micro Raman spectrometer with 514.12 nm laser source.

## 3 Results and discussion

### 3.1 Structural studies

Figure 1 shows HRXRD pattern of the ZnSe thin films stacked with various PbSe ML thickness ranges from 2.5 to 10 nm. A typical polycrystalline nature of the material was inferred from the shape of the peaks. All the samples

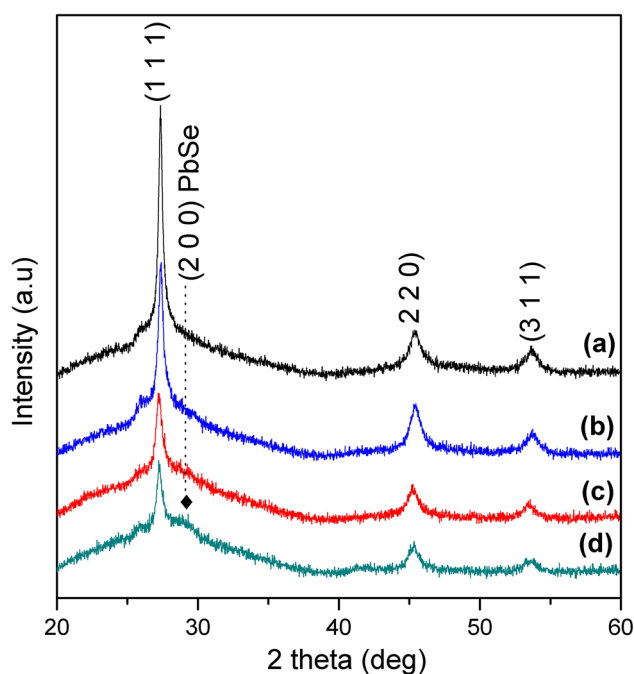


**Fig. 1** HRXRD pattern of ZnSe thin films stacked with PbSe ML with various thicknesses, *a* 2.5 nm, *b* 5 nm, and *c* 10 nm. The arrow symbols represent evaluation of PbSe crystallographic phases

exhibit dominant Bragg reflection at about  $27.3^\circ$  corresponding to (1 1 1) plane of cubic Zinc blende structure. Two other peaks are observed at about  $45.5^\circ$  and  $53.8^\circ$  corresponding to (2 2 0) and (3 1 1) planes also associated with crystallographic planes of cubic ZnSe. This observation matches with the earlier works [5, 7] and standard JCPDS values (card no: 70-0777) for the space group of  $Fm\bar{3}m$  and lattice parameter of 5.670 Å. However, the position of these peaks is slightly shifted to lower angles with increasing PbSe ML thickness from 2.5 to 10 nm and are listed in Table 1. It can be noteworthy to state that the intensity of the (1 1 1) peak decreases with increasing PbSe ML thicknesses which might be due to evaluation of PbSe phase. One can see that ZnSe with 10 nm thick PbSe shows evaluation of diffraction peaks at  $25.6^\circ$ ,  $29.2^\circ$ , and  $41^\circ$  indicated by  $\blacklozenge$  symbol in Fig. 1. These peaks are associated with crystallographic phases of PbSe corresponding to (1 1 1), (2 0 0), and (2 2 0) planes, respectively (JCPDS: 78-1903). From this, one can conclude that the shift in ZnSe orientation towards lower angle side indicates increasing tensile strain in the ZnSe layers due to increase in PbSe ML thickness [15]. The average crystalline size was calculated using Debye–Scherrer’s formula [15],

$$D = \frac{k\lambda}{\beta \cos \theta} \quad (1)$$

where  $k$  is the shape factor that was taken equal to 0.9,  $\lambda$  is the wavelength of X-ray used (1.54 Å),  $\beta$  is the full width

**Table 1** Structural parameters of ZnSe stacked with 2D layers of PbSe ML with various thicknesses

Thickness of PbSe ML (nm)	2θ (°)	FWHM (β)	d-spacing	Crystalline size (D) (nm)	Lattice constant (a) (Å)	Micro strain (ε) × 10 <sup>-3</sup>
2.5	27.3259	0.3887	3.2598	21	5.64	1.64
5.0	27.2911	0.4015	3.2638	20	5.65	1.70
10	27.1363	0.4201	3.2821	19	5.68	1.78

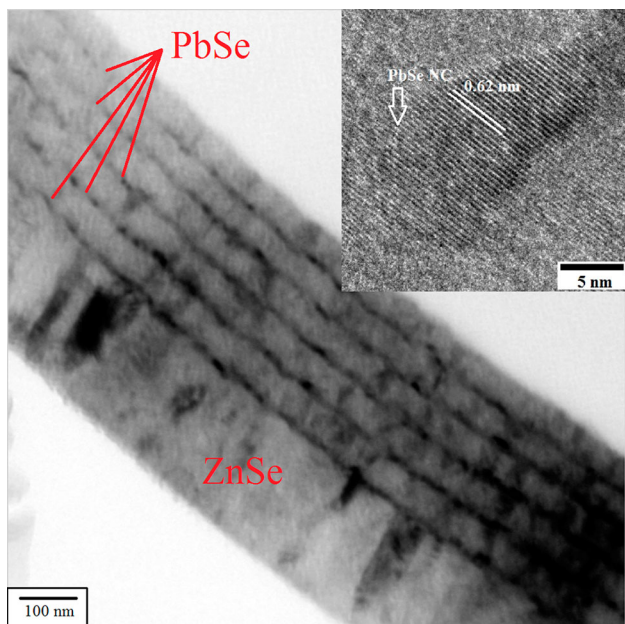


**Fig. 2** Bright field cross-sectional TEM image of ZnSe-PbSe ML thin film. Light and dark contrast of the image indicates ZnSe and PbSe layers, respectively. Lattice fringes of the PbSe layer are shown as a magnified view in inset of the figure

half maximum (FWHM) of the peak and θ is the Bragg diffraction angle. The lattice constant (a) of ZnSe-PbSe thin films for its cubic crystal structure was determined using the relation,

$$\frac{1}{d^2} = \frac{h^2 + k^2 + l^2}{a^2} \tag{2}$$

where (h k l) are the Miller indices and d is the d-spacing of the peak. It is more likely that micro strain is one of the causes of shift in Bragg peak position in ZnSe-PbSe ML due to heap arrangement. The micro strain developed in the ZnSe-PbSe ML was calculated using the relation [15],

$$\left(\frac{\beta \cos \theta}{\lambda}\right)^2 = \frac{1}{d^2} + 16\epsilon^2 \left(\frac{\sin \theta}{\lambda}\right)^2 \tag{3}$$

where ‘ε’ is the presence of micro strain in ZnSe-PbSe ML structure.

The calculated structural parameters of ZnSe-PbSe ML thin films with different thicknesses are listed in Table 1.

The estimated lattice constant value for all the samples is nearly same which indicates PbSe ML does not disturb the lattice parameters of ZnSe. From the Table 1, it is evident that PbSe ML increases the micro strain at ZnSe-PbSe which results in shift in the Bragg peak position. However, no significant changes in FWHM and corresponding crystalline size of (1 1 1) oriented ZnSe thin films observed since all the structures have the same ZnSe thickness architecture.

Figure 2 shows the bright field cross-sectional TEM image of ZnSe thin film stacked with 10 nm thick PbSe ML. A good periodicity and ordering of the ZnSe-PbSe layered structure can be seen in the TEM image. In the structure, the material formation is evident through a dark and lighter feature. The dark and lighter contrasts are associated to the PbSe layers and ZnSe layers, respectively. The thickness of the PbSe and ZnSe is consistent throughout as predicted based upon the rate of evaporation during sample preparation. Inset shows magnified view of the image focussing on PbSe layer. The lattice fringes in PbSe layer evident that ML = 10 nm has crystalline PbSe layers in consistent with XRD pattern.

### 3.2 Optical studies

Figure 3 depicts optical absorption spectra of ZnSe stacked with PbSe ML along with reference ZnSe thin film. It can be noted that upon stacking of PbSe ML, the absorption onset significantly red shifted in response with reference ZnSe film. It is noteworthy to state that the absorption edges of all the samples start with nearly same wavelength (330 nm) alluding that ZnSe play a major role to absorb the energy in visible region. A broad absorption region has observed upon the insertion of PbSe ML in comparison with reference ZnSe thin film. It is well known that one of the next generation solar cell research focus on utilizing broad solar spectrum. In the present work, wide band gap ZnSe absorbs the energy in the visible region, whereas quantum confined 2D PbSe ML actively provides complementary NIR absorption to ZnSe results full solar spectrum utilization. However, more optimization needs to use PbSe as active NIR absorbing layers and confirm the exciton creation in NIR region. The fundamental absorption edge in most chalcogenide follows an exponential law.

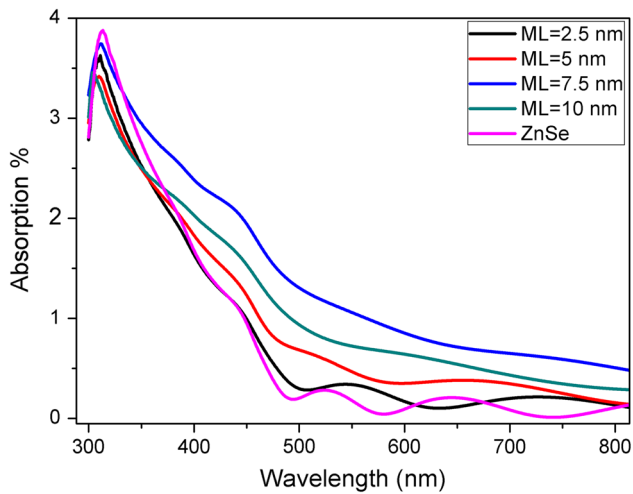


**Fig. 3** Optical absorption spectra of ZnSe-PbSe ML thin films with various PbSe ML thicknesses along with reference ZnSe spectrum

Above the exponential tail, the absorption coefficient has been reported to obey the following relation [16],

$$\alpha(h\nu) = d^{-1} \ln \left( \frac{h\nu}{A} \right)^{-1} \quad (4)$$

where 'd' is the thickness of the samples. Then the band gap energy ( $E_g$ ) can be deduced from the relation [16],

$$(\alpha h\nu)^2 = A(h\nu - E_g)^n \quad (5)$$

where 'A' is a constant which arises from Fermi's golden rule for fundamental band-to-band electronic transition and exponent  $n = 1/2$  for direct allowed transition. Figure 4 shows the variation curves of  $(\alpha h\nu)^2$  as a function of photon energy ( $h\nu$ ) for ZnSe-PbSe ML thin films. The  $E_g$  of the ZnSe-PbSe films was determined by extrapolating the

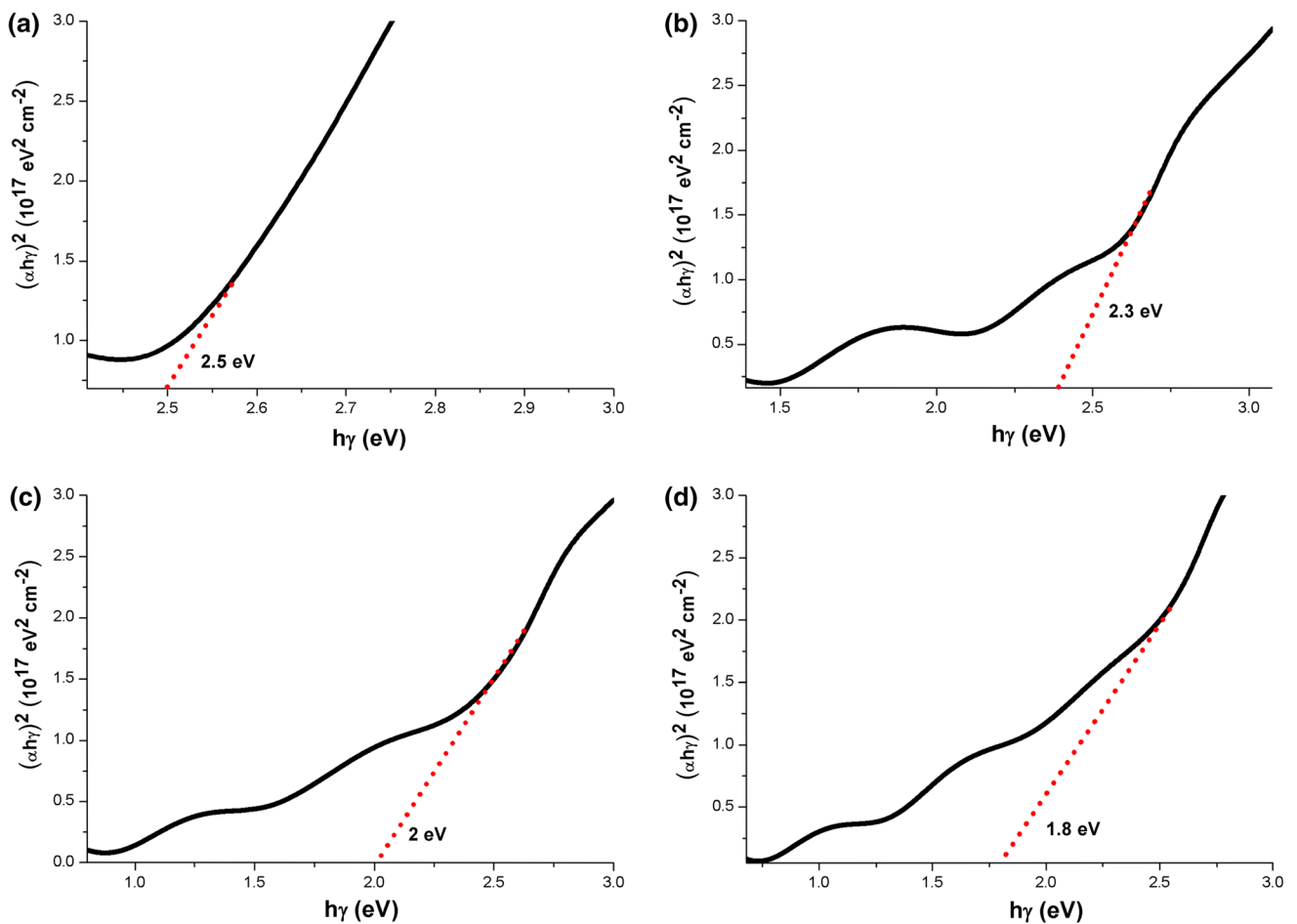


**Fig. 4** Band gap plot of  $(\alpha h\nu)^2$  as a function of photon energy ( $h\nu$ ) for ZnSe-PbSe ML thin films with PbSe ML thickness for, **a** 2.5 nm, **b** 5 nm, **c** 7.5 nm, and **d** 10 nm

linear portion of the curve to the energy axis at  $(\alpha h\nu)^2 = 0$ . The  $E_g$  decreases with increasing PbSe ML thicknesses as observed in the optical absorption spectra (Fig. 3). The obtained band gap energies lie between 2.5 and 1.8 eV. It is noteworthy to state that the couple of short range linear regions, the so-called sub band energy levels are observed in the continuum of the absorption coefficient tail. This behaviour might be associated with quantum confined 2D PbSe ML due hole confinement [17]. The  $E_g$  of reference ZnSe shows a uniform linear region, whereas in the plot of ZnSe–PbSe shows discrete energy level which indicates the capability to absorb the energy in wide range of solar spectrum.

Impact of PbSe ML on the complementary NIR absorption of ZnSe was confirmed by photoluminescence (PL) emission to support the absorption studies. Figure 5 shows the room temperature PL spectra of ZnSe stacked with 10 nm PbSe ML excited at 532 nm continuous laser source. The spectrum was fitted with Lorentz curve (dashed line) for clarity and shows a well-resolved emission peak with a shoulder peak. A strong emission at 1,071 nm is due to the radiative recombination of electrons localized at excited ( $1E_s$ ) state and the shoulder-like peak at 1,085 nm is assigned to be ground ( $G_s$ ) states of PbSe. Similar result of PbSe emission has been reported for 2.8 nm PbSe nanocrystals in ZnO/PbSe heterostructure interfaces [18].

### 3.3 Raman scattering

One of the effective ways to study the stress and strain-induced quantum size effect or interfacial effect in semiconductor is Raman scattering [19]. Figure 5 shows Raman spectra of ZnSe–PbSe along with reference ZnSe thin film.

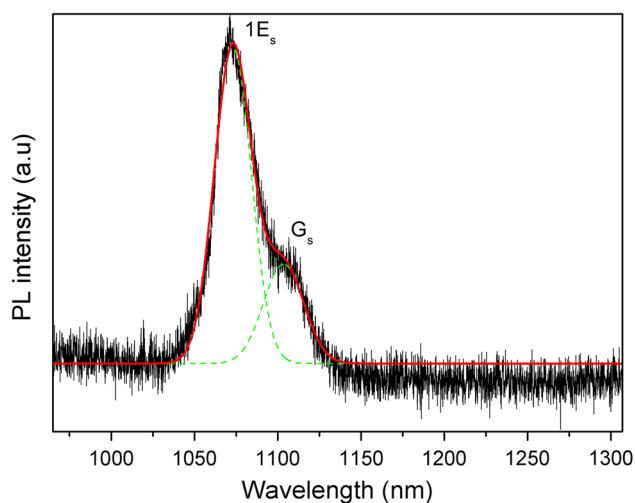


**Fig. 5** Photoluminescence spectra of ZnSe stacked with 10 nm PbSe ML excited at 532 nm laser source. Lorentz fit of the spectra is indicated by dashed lines

Inset shows the vibrational Raman spectra of reference PbSe thin film. Raman spectra of reference ZnSe show first and second order Longitudinal Optical (LO) phonons besides Transverse Optical (TO) phonon located at 252, 504 and 204  $\text{cm}^{-1}$ , respectively [20]. Raman spectra of reference PbSe show first (128  $\text{cm}^{-1}$ ) and second (138  $\text{cm}^{-1}$ ) order LO phonon modes with ground state energy polaron located at 790  $\text{cm}^{-1}$ . When a crystal is under compression or tension, the optical phonon modes are shifted upward or downward compared to its bulk phonon mode [21]. In the spectra of ZnSe–PbSe ML, the 1LO and 2LO phonon modes are shifted downward in response to reference ZnSe and disposed between the frequencies of the 1LO mode of ZnSe (252  $\text{cm}^{-1}$ ) and 2LO mode of PbSe (238  $\text{cm}^{-1}$ ). The LO band is asymmetric and has quite large FWHM, which has been related to lattice distortion due to interface between ZnSe and PbSe. In addition, an evaluation of 1LO like PbSe optical phonon modes are observed in ZnSe–PbSe ML indicates crystalline nature of the PbSe layers. As can be seen in Fig. 6 that TO mode of ZnSe decreases for 2.5 nm ML and vanishes for 10 nm PbSe ML which indicates ZnSe crystals are randomly oriented on the surface. Since no compositional changes in ZnSe in all the structures, one can relate blue-shift in optical band gap energy to an increase of internal strain in the ZnSe layers with decreasing PbSe layer thickness. It is also seen from Fig. 4 that the intensity of the scattered light is high for 2.5 nm PbSe layer thickness which is by the factor of  $\sim 2$  in comparison with 10 nm ML. This observed effect is possibly manifestation of resonance enhancement of the Raman scattering when the energy of the incident light approaches the optical band gap. It is well known that disorder in semiconductor system results evaluation of new vibrational modes. New

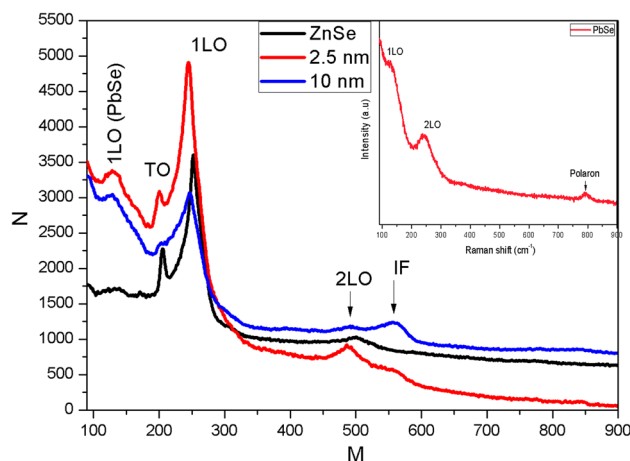


**Fig. 6** Raman spectra of ZnSe–PbSe ML thin films along with reference ZnSe spectrum. Inset shows vibrational spectrum of reference PbSe thin film

vibrational modes at  $560\text{ cm}^{-1}$  in ZnSe–PbSe ML are attributed to the interfacial (IF) phonon mode [22] which needs further study for the explanation of the new features.

#### 4 Conclusion

Structural and optical properties of thermally evaporated ZnSe thin films stacked with PbSe ML at different thickness ranges from 2.5 to 10 nm have been studied. The typical polycrystalline nature of the material was inferred from the shape of the peaks and its structural parameters were reported. Increases of micro strain development at the interfaces of ZnSe with increasing PbSe ML thickness were observed. A good periodicity and well-ordered PbSe ML at the interfaces of ZnSe were seen through a cross-sectional TEM image. Enhanced optical absorption from UV to NIR region was observed upon stacking of PbSe ML. The obtained band gap values are laid between 1.8 and 2.5 eV with sub band gaps at NIR region show the possibilities for full solar spectrum utilization. A downward shift in ILO like ZnSe optical phonon mode indicates the presence of tensile strain the ZnSe layers along with evaluation of ILO like PbSe phonon mode in stacked ZnSe–PbSe ML thin films.

**Acknowledgments** Authors acknowledge the research council of Norway for providing Yggdrasil mobility grant (Project No: 219721/F11) to carry out TEM analysis at TEM Gemini centre, Norwegian University of Science and Technology, Norway. We extend our grateful to CRF, IIT Kharagpur and Department of Nanoscience and Technology, Bharathiar University for HRXRD and Raman measurements respectively.

#### References

1. D. Yun, W. Feng, H. Wu, K. Yoshino, *Sol. Energy Mat. Sol. Cell* **93**, 1208 (2009)

2. H. Wenisch, M. Fehrer, M. Klude, K. Ohkawa, D. Hommel, *J. Cryst. Growth* **214–215**, 1075 (2000)
3. S.P. Nehra, M. Singh, *Vacuum* **85**, 719 (2011)
4. A.P. Samantilleke, M.H. Boyle, J. Young, I.M. Dharmadasa, *J. Mater. Sci. Mater. Electron.* **9**, 231 (1998)
5. X. Wang, J. Zhu, Y.G. Zhang, J. Jiang, S. Wei, *Appl. Phys. A* **99**, 651 (2010)
6. S. Abe, *Nanoscale Res. Lett.* **6**, 324 (2011)
7. S. Venkatachalam, D. Mangalaraj, S.K. Narayandass, S. Velumani, P. Schabes-Retchkiman, J.A. Ascencio, *Mater. Chem. Phys.* **103**, 305 (2007)
8. T.K. Lin, S.J. Chang, Y.K. Su, Y.Z. Chiou, C.K. Wang, S.P. Chang, C.M. Chang, J.J. Tang, B.R. Huang, *Mater. Sci. Eng. B* **119**, 202 (2005)
9. J. Ren, K.A. Bowers, B. Sneed, F.E. Reed, J.W. Cook Jr, J.F. Schetzina, *J. Cryst. Growth* **111**, 829 (1991)
10. S. Miwa, L.H. Kuo, K. Kimura, A. Ohtake, T. Yasuda, C.G. Jin, T. Yao, *J. Cryst. Growth* **184–185**, 41 (1998)
11. H.Q. Jiang, X. Yao, J. Che, X. Wan, M.Q. Wang, *J. Electroceram.* **21**, 733 (2008)
12. B. Pejova, B. Abay, I. Bineva, *J. Phys. Chem. C* **114**, 15280 (2010)
13. J.M. Luther, M.C. Beard, Q. Song, M. Law, R.J. Ellingson, A.J. Nozik, *Nano Lett.* **7**, 1779 (2007)
14. Y. Masumoto, H. Takagi, H. Umino, E. Suzumura, *App. Phys. Lett.* **100**, 252106 (2012)
15. Thad Vreeland Jr, Bruce M. Paine, *J. Vac. Sci. Technol.* **A4**(6), 3153 (1986)
16. J. Tauc, *Amorphous and Liquid Semiconductors* (Plenum press, New York, 1979)
17. B. Pejova, I. Grozdanov, *Mater. Chem. Phys.* **90**, 35 (2005)
18. C.F. Cai, B.P. Zhang, R.F. Li, H.Z. Wu, T.N. Xu, W.H. Zhang, J.F. Zhu, *Europhys. Lett.* **99**(3), 37010 (2012)
19. C. Raptis, D. Nesheva, Y.C. Boulmetis, Z. Levi, Z. Aneva, *J. Phys. Condens. Mater.* **16**, 8221 (2004)
20. G. Perna, M. Lastella, M. Ambrico, V. Capozzi, *Appl. Phys. A* **83**, 127 (2006)
21. D. Nesheva, M. Scepanovic, Z. Aneva, Z. Levi, Z.V. Popovic, I. Miloushev, *Phys. Status Solidi A* **209**, 949 (2012)
22. N. Garro, A. Cros, J.M. Llorens, A. Garcia-Cristobal, A. Cantarero, N. Gogneau, E. Sarigiannidou, E. Monroy, B. Daudin, *Phys. Rev. B* **74**, 075305 (2006)